


A tunable Doppler-free dichroic lock for laser frequency stabilization

Vivek Singh¹  · V. B. Tiwari¹ · S. R. Mishra¹ · H. S. Rawat¹

Received: 25 April 2016 / Accepted: 19 July 2016 / Published online: 4 August 2016
© Springer-Verlag Berlin Heidelberg 2016

Abstract We propose and demonstrate a laser frequency stabilization scheme which generates a dispersion-like tunable Doppler-free dichroic lock (TDFDL) signal. This signal offers a wide tuning range for lock point (i.e. zero-crossing) without compromising on the slope of the locking signal. The method involves measurement of magnetically induced dichroism in an atomic vapour for a weak probe laser beam in the presence of a counter-propagating strong pump laser beam. A simple model is presented to explain the basic principles of this method to generate the TDFDL signal. The spectral shift in the locking signal is achieved by tuning the frequency of the pump beam. The TDFDL signal is shown to be useful for locking the frequency of a cooling laser used for magneto-optical trap (MOT) for ^{87}Rb atoms.

1 Introduction

Laser frequency stabilization is an essential requirement for various applications including atom cooling [1], high resolution spectroscopy [2], precision measurements [3] etc. A setup for laser cooling and trapping of atoms requires several lasers which are actively frequency stabilized and locked at few linewidths detuned from the peak of atomic absorption. In the laser cooling experiments, the active frequency stabilization is achieved by generating a reference signal which is based on absorption profile of atom around the resonance. The reference locking signal

can be either Doppler-broadened with wide tuning range or Doppler-free with comparatively much steeper slope but with limited tuning range. The simplest technique for frequency locking involves locking to the side of the Doppler-free peak generated from the saturated absorption spectroscopy (SAS) [4, 5]. However, the SAS technique is sensitive to the intensity fluctuations in laser beam due to intensity-dependent broadening in SAS signal. The locking of the laser frequency to the peak of an atomic reference signal such as in frequency modulated spectroscopy (FMS) [6] provides high signal-to-noise ratio (SNR) but needs dithering of laser frequency and a phase sensitive detection system. A suitable dispersion-like reference signal for peak locking can be generated using polarizing spectroscopy (PS) [7–11] without frequency modulation and phase sensitive detection. Along with these techniques, there are also methods for laser frequency stabilization which employ PS with the external magnetic field [12, 13]. However, the techniques involving polarization spectroscopy are sensitive to the surrounding stray magnetic field [14]. An alternative technique which can generate narrow dispersion-like reference signal exploits circular dichroism of an atomic vapour in the presence of a magnetic field. In this technique, the difference of Zeeman shifted saturated absorption signals generates the Doppler-free dichroic lock (DFDL) signal [15–24]. This technique requires only low magnetic field for its operation and is less sensitive to the surrounding stray magnetic field. Also being a difference-based technique, it is less sensitive to fluctuations in laser beam intensity. However, the tuning range of this technique is limited to few natural linewidths of the transition. The tuning range can be increased by electronically adding an offset voltage to the signal or by optically changing the quarter wave plate axis relative to the polarization beam splitter axis [16].

✉ Vivek Singh
viveksingh@rrcat.gov.in

¹ Laser Physics Applications Section, Raja Ramanna Centre for Advanced Technology, Indore 452013, India

The locking range can also be extended by either using Doppler-broadened version of this technique known as dichroic atomic vapor laser lock (DAVLL) [25–28] signal or by locking at positive as well as the negative slopes of DFDL signal [16]. Another method involves increasing the magnetic field [29] to extend the locking range of the DFDL signal. This frequency tuning is often achieved by compromising the slope of the signal which is a crucial parameter for the frequency locking. A recently reported study on DFDL spectroscopy of D-2 line of ^{87}Rb includes the coherence for the calculation of line-shape of the real atomic system [30].

Here, we present a technique which generates a narrow tunable DFDL (TDFDL) signal without compromising with the slope of the signal. The frequency tuning of this dispersion-like TDFDL signal is achieved by varying the pump laser frequency using AOMs. We have studied the dependence of this frequency locking signal’s amplitude and the slope on various experimental parameters such as the pump beam power and the magnetic field. The locking performance of an extended cavity diode laser (ECDL) system is investigated by measuring the change in the number of cold atoms in a magneto-optical trap (MOT). A simple theoretical model to explain the generation of TDFDL signal is also presented.

2 Theoretical analysis

We adopt a simple two-level system involving hyperfine energy levels to explain the generation of TDFDL signal. A linearly polarized weak probe beam is overlapped by a counter-propagating strong pump beam in an atomic vapour cell placed in a weak magnetic field. The propagation of the probe beam is along the axis of magnetic field. The linearly polarized light can be resolved into two counter-rotating circular components σ_{\pm} using quarter wave plate and polarizing beam splitter. In the absence of magnetic field ($B=0$), different $m_{F'}$ states are degenerate and hence, σ_{+} and σ_{-} transitions overlap. When a small magnetic field (few Gauss) is applied, the degeneracy is lifted and medium becomes dichroic due to the displacement of σ_{+} and σ_{-} transitions. As a result, the pair of spectrally shifted saturated absorption spectroscopy (SAS) signals on subtraction generates the Doppler-free dispersion-like signal[29]. For atoms moving with velocity \mathbf{v} , the Doppler shifted laser frequency in the frame of moving atom becomes $\omega' = \omega_0 - \mathbf{k}\cdot\mathbf{v}$. When the laser beam passes through a Rb atomic sample with a Maxwell–Boltzmann velocity distribution, only those atoms which fall within the homogeneous linewidth Γ around the centre frequency ω_0 of Rb atom at rest can significantly contribute to the absorption (Fig. 1).

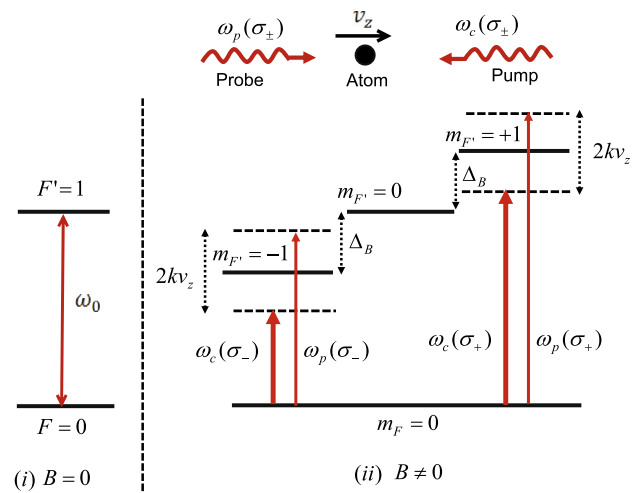


Fig. 1 Schematic diagram showing resonant interaction of σ_{+} and σ_{-} polarized pump and the probe beams when a weak magnetic field is applied to an atom having lower level $F = 0$ and upper level $F' = 1$ is in motion

If the pump beam having frequency (ω_c) and the probe beam having frequency (ω_p) are in counter-propagating directions, the atoms having velocity components of v_z along the direction of the probe beam see different values of the frequency detunings with the pump and the probe beams in the presence of magnetic field. The σ_{\pm} polarized pump and the probe beams can interact resonantly with this group of atoms if,

$$\omega_p(\sigma_{\pm}) - kv_z = \omega_0 \pm \Delta_B \tag{1}$$

$$\omega_c(\sigma_{\pm}) + kv_z = \omega_0 \pm \Delta_B \tag{2}$$

Using Eqs. (1) and (2), the relation between the probe beam detuning $\Delta_p^{\pm} = \omega_p(\sigma_{\pm}) - \omega_0$ and the pump beam detuning $\Delta_c^{\pm} = \omega_c(\sigma_{\pm}) - \omega_0$ for resonant interaction is given by

$$\Delta_c^{\pm} + \Delta_p^{\pm} = \pm 2\Delta_B \tag{3}$$

Again using Eqs. (1) and (2), the difference between the pump and the probe beam detunings is given by,

$$\Delta_{cp} = \Delta_c^{\pm} - \Delta_p^{\pm} = -2kv_z \tag{4}$$

Using Eqs. (3) and (4), resonance condition for σ_{\pm} probe beam in the presence of the counter-propagating pump beam and the applied magnetic field can be written as

$$\Delta_p^{\pm} = -\frac{\Delta_{cp}}{2} \pm \Delta_B \tag{5}$$

Therefore, the probe absorption signal will depend upon the difference between the pump and the probe beams detunings and the applied magnetic field.

In the case of simple model, $F = 0 \rightarrow F' = 1$, the absorption cross section for σ_{\pm} probe beam for an atom with velocity component v_z is given as[4]

$$\rho_{\pm}(\Delta_p^{\pm}, v_z) = \frac{\rho_0(\Gamma/2)^2}{(\Delta_p^{\pm} \mp \Delta_B - kv_z)^2 + (\Gamma/2)^2} \quad (6)$$

where ρ_0 is the maximum absorption cross section at $\Delta_p^{\pm} = \pm\Delta_B + kv_z$, $\Delta_B = \mu_B B g_{F'} m_{F'}/\hbar$ (for $F = 0 \rightarrow F' = 1$ case) is Zeeman splitting of the levels in magnetic field, k is the wave vector of laser light.

Due to pump laser beam (ω_c), population density in ground state ($F = 0$ level) decreases within the velocity interval $dv_z = \frac{\Gamma}{k}$, while population density in magnetically shifted upper level ($F' = \pm 1$ level) increases. Therefore, population in the lower level after pump has caused excitation from lower level is given by

$$\Delta N(\Delta_c^{\pm}, v_z) = N^0(v_z) \left[1 - g_1 \frac{(\Gamma/2)^2}{(\Delta_c^+ - \Delta_B + kv_z)^2 + (\Gamma/2)^2} - g_2 \frac{(\Gamma/2)^2}{(\Delta_c^- + \Delta_B + kv_z)^2 + (\Gamma/2)^2} \right] \quad (7)$$

where Γ is a natural linewidth for $F = 0 \rightarrow F' = 1$ transition, g_1 and g_2 are coefficients representing the depth of dips burnt in the distribution by the pump beam and depend on the pump beam intensity used. For our calculations, we have assumed $g = g_1 = g_2$. The population in the ground state with velocity range v_z and $v_z + dv_z$ from where probe makes the absorption transition is given as

$$N^0(v_z)dv_z = C \exp[-(v_z/v_p)^2] dv_z \quad (8)$$

where v_p is the most probable velocity, and C is a constant depending on number of atoms in gas, density etc.

The absorption coefficient for a weak probe laser beam in the presence of the pump beam is given by

$$\alpha_{\pm}(\Delta_p^{\pm}, \Delta_c^{\pm}) = \int_{-\infty}^{\infty} \rho_{\pm}(\Delta_p^{\pm}, v_z) \Delta N(\Delta_c^{\pm}, v_z) dv_z \quad (9)$$

The integration in (9) can be performed over velocity and assuming the Doppler width, $\Delta_D \gg \Gamma$ (where $\Delta_D = kv_p$) to obtain α_{\pm} values.

For low optical density of the sample, the dichroic signal (DS) generated by TDFDL technique can be given as

$$DS(\Delta_p^{\pm}, \Delta_c^{\pm}) = \alpha_+(\Delta_p^+, \Delta_c^+) - \alpha_-(\Delta_p^-, \Delta_c^-) \quad (10)$$

Using Eqs. (7), (8) and (9), the TDFDL signal is

$$DS(\Delta_p^{\pm}, \Delta_c^{\pm}) = C[(D_+ - D_-) - g(D_+L_+ - D_-L_-)] \quad (11)$$

where $D_{\pm} = \frac{1}{\sqrt{\pi}} \exp[-((\Delta_p^{\pm} \mp \Delta_B)/\Delta_D)^2]$

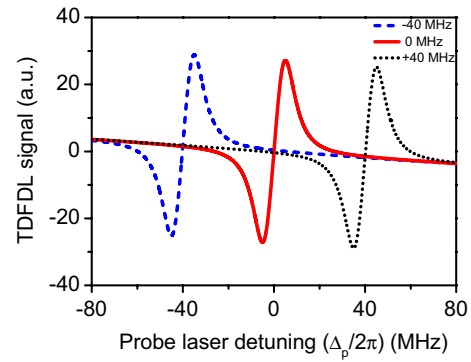


Fig. 2 Calculated TDFDL signals $DS(\Delta_p^{\pm}, \Delta_c^{\pm})$ (using Eq. (11)) for the parameter $\Delta_D = 50\Gamma$, $C = 1$, $g = 0.04$, $m_F = 0$, $g_{F'} = 2/3$, $m_{F'} = 1$, $\Gamma/2\pi = 12$ MHz, $B = 4$ G and $\Delta_{cp}/2\pi = +80, 0$ and -80 MHz corresponds to dashed line, solid line and dotted line, respectively

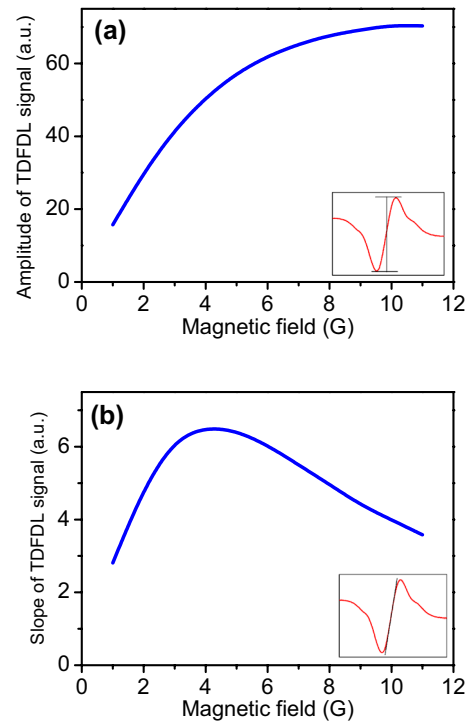


Fig. 3 Calculated dependence of **a** amplitude and **b** Slope of TDFDL signal on magnetic field. $\Delta_D = 50\Gamma$, $\Gamma/2\pi = 12$ MHz, $C = 1$, $g = 0.04$, $m_F = 0$, $g_{F'} = 2/3$, $m_{F'} = 1$ and $\Delta_{cp}/2\pi = +24$ MHz

$$L_{\pm} = \frac{\Gamma^2}{(\Delta_p^{\pm} + \Delta_c^{\pm} \mp 2\Delta_B)^2 + (2\Gamma/2)^2}$$

L_{\pm} can be written in terms of Δ_{cp} using equation (4),

$$L_{\pm} = \frac{(\Gamma/2)^2}{(\Delta_p^{\pm} + \frac{\Delta_{cp}}{2} \mp \Delta_B)^2 + (\Gamma/2)^2}$$

The signal consists of two parts: the first part represents a Doppler-broadened dichroic signal. The second part appears due to the presence of pump beam, and it is represented by two Doppler-free absorption coefficients of σ_+ and σ_- components.

Figure 2 shows the calculated TDFDL signal for different pump laser detuning. As the pump laser frequency is blue detuned with respect to the probe beam, the zero-crossing in dispersion-like TDFDL signal will be shifted to the red and vice versa. Therefore, the zero-crossing in the TDFDL signal can be shifted to any frequency depending upon the pump laser detuning.

Further, Fig. 3a, b shows the calculated amplitude and the slope of the TDFDL signal (12 MHz red detuned) with the axial magnetic field, respectively. We find that the amplitude (difference of maximum and minimum values) of the TDFDL signal initially increases with the applied magnetic field and gets saturated after certain value of the magnetic field. The amplitude of TDFDL signal reaches maximum value when SAS for σ_+ and σ_- probe beams is just separated by increasing the magnetic field. Further, the slope of the TDFDL signal increases with magnetic field and reaches the maximum value at magnetic field of ~ 4 Gauss as shown in Fig. 3b. The slope starts to decrease with further increase of the magnetic field due to increased separation between σ_+ and σ_- probe laser beam signals.

3 Experimental setup

The TDFDL experimental setup is shown in Fig. 4. The external cavity diode laser (ECDL) (DL100, Toptica) system operating at 780 nm is used in our experiments. A combination of half wave plate and polarizing beam splitter (PBS) is used to suitably divide the laser output beam for its use in the TDFDL setup, a reference SAS setup and a magneto-optical trap (MOT) setup.

In the TDFDL setup, laser light is split in two parts, namely, the pump laser beam and the probe laser beam using the combination of half wave plate and PBS. The pump laser beam is passed through a setup of two acousto-optical modulators (AOMs), AOM-1 and AOM-2 having frequency range of 60–100 MHz. The pump laser beam is initially passed through AOM-1. The first-order (+1) diffracted beam of AOM-1 is retro-reflected and passed again through AOM-1 before going to pass through the second AOM, i.e. AOM-2 (Fig. 4). In AOM-2, the first order (−1) is made retro-reflected. Thus, we have used both the AOMs in double pass configuration to avoid deviation of the output beam. The output pump beam is overlapped with the probe laser beam in counter-propagating direction inside a 5-cm long Rb vapour cell placed inside the solenoid with crossing of ~ 10 mrad. In the TDFDL setup, the pump

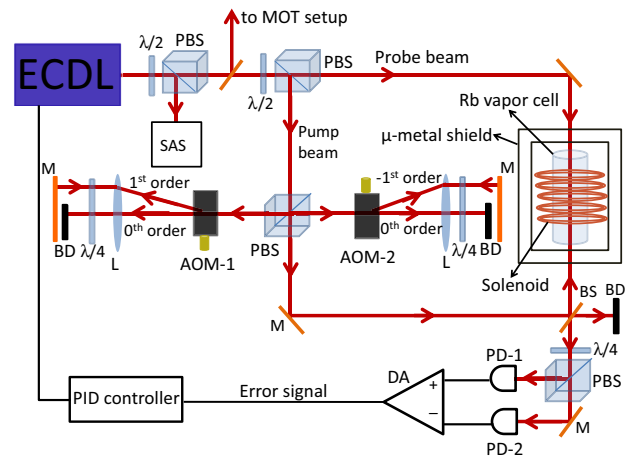


Fig. 4 Schematic diagram of the TDFDL spectroscopy setup. ECDL external cavity diode laser, MOT magneto-optical trap, PBS polarizing beam splitter, BD beam dump, BS beam splitter, AOM acousto-optic modulator, DA differential amplifier, PD photodiode, SAS saturated absorption spectroscopy, M mirror, L lens, $\lambda/4$ quarter wave plate, $\lambda/2$ half wave plate. Two detectors (PD-1 and PD-2) monitor the absorption of light which has driven σ_+ and σ_- transitions

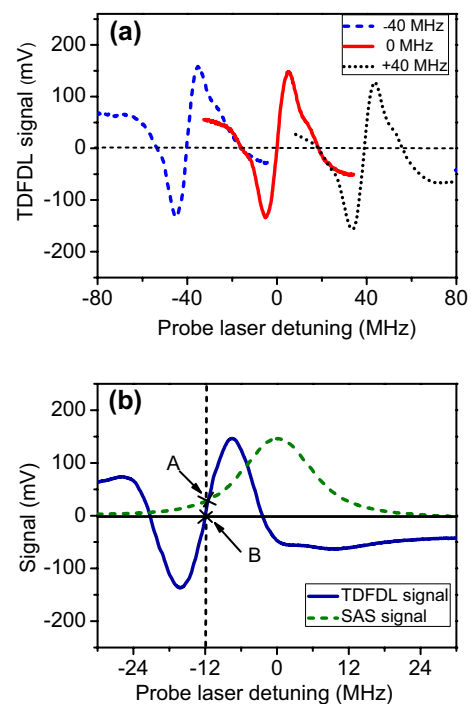


Fig. 5 a Observed spectral shift of the TDFDL signal for $F = 2 \rightarrow F' = 3$ transition of ^{87}Rb atom for $\Delta_{\text{AOM}}/2\pi = +80, 0$ and -80 MHz (dashed curve, solid curve and dotted curve, respectively). b TDFDL signal at -12 MHz detuning with reference to SAS signal. Slope of SAS signal is ~ 6 mV/MHz at point A, whereas the slope of TDFDL signal is ~ 43 mV/MHz at point B. pump power = 1.13 mW, Probe power = $140\mu\text{W}$, and magnetic field = 9.7 G for the data in figure (b)

beam passes through two PBSs before entering into the Rb vapour cell. Therefore, the pump beam power due to imperfect polarization is very small ($\sim 0.1\%$) and has not produced any observable adverse effects on the TDFDL signal. The probe laser beam is monitored using a $\lambda/4$ wave plate and a PBS combination of elements and photodiodes for detection of σ_+ and σ_- parts of polarizations (Fig. 4). The difference of two photodiode signals gives dispersion-like signal. The solenoid generates the longitudinal field of ~ 32 G/A. At the Rb vapour cell, the probe and the pump laser beam has a diameter of 3 mm. Neutral density filters are used to vary the pump laser beam power.

4 Results and discussions

4.1 Frequency tuning of the TDFDL spectra using AOMs

The frequency tuning of the TDFDL signal is achieved by varying the frequency of the pump laser beam with the help of two AOMs in double pass configuration as shown in Fig. 4. The pump laser beam after double pass through AOM-1 gets a frequency shift of $2\omega_1$, where ω_1 is shift in first-order diffraction in AOM-1. When this first-order diffracted beam passes through AOM-2, the frequency shift is $-2\omega_2$, where ω_2 is shift in first order in AOM-2. Therefore, the frequency of the pump beam is shifted by Δ_{AOM} ($\Delta_{AOM} = 2(\omega_1 - \omega_2) = \Delta_{cp}$, relative to the probe beam frequency. Therefore, as we observed, (Fig. 5a), there is no spectral shift in the TDFDL signal when AOM-1 and AOM-2 operate at the same frequency. This is because, the pump and the probe laser beam will be interacting with zero velocity group resulting a TDFDL signal as shown in Fig. 5a (solid curve). Further, if the AOM-1 and AOM-2 operate at frequency 100 and 60 MHz, respectively, then frequency shift of the pump beam ($\Delta_{AOM}/2\pi$) as compared to the probe beam becomes +80 MHz. Therefore, the TDFDL signal will be red shifted (-40 MHz) as shown by dashed curve in Fig. 5a. In the same way, the TDFDL signal can be shifted to the blue detuned ($+40$ MHz), as shown by the dotted curve in Fig. 5a, if AOM-1 and AOM-2 operate at the frequency of 60 and 100 MHz, respectively. Thus, observed detuning behaviour of the TDFDL signal shown in Fig. 5a is in good qualitative agreement with the theoretically calculated signal as shown in Fig. 2. However, the reason for difference in the slope of signals shown in Figs. 2 and 5a is perhaps due to multiple levels involved in actual experimental situation. This gives rise to many dispersive TDFDL signals (corresponding to other transitions) adjacent to the signal shown in Fig. 5a.

We have also observed that the slope and the amplitude of the signal remains nearly unchanged throughout the

whole tuning range. Thus, the frequency stability achieved using the TDFDL reference signal is expected to be nearly independent of the frequency shifting used. This is the qualitatively different from the SAS signal where the slope and the amplitude changes with detuning from the resonance peak. It is shown in Fig. 5b that the slope of the TDFDL signal is ~ 43 mV/MHz, whereas as the slope of SAS signal is ~ 6 mV/MHz at -12 MHz detuning. The advantage of TDFDL technique is, thus, obvious due to higher slope of the signal and its less sensitivity towards laser beam intensity fluctuations. Here, we note that the relative difference in the detuning of the pump and the probe beams can also be introduced using two different lasers as reported in ref. [11]. However, in that case, the locking performance of one laser may influence the frequency stabilization of the other laser. We note that the tuning of the laser frequency using a DF DL setup can also be achieved by changing the frequency of the final laser beam using AOMs. But this may be an inefficient method due to loss of power through AOMs used in the final beam.

4.2 Dependence of the TDFDL spectra on the magnetic field strength and the pump laser beam power

This TDFDL signal is utilized to lock the laser frequency at zero-crossing point of the signal. The lock stability of laser is dependent on peak-to-peak amplitude and slope of the TDFDL signal at the zero-crossing position. Therefore, dependence of peak-to-peak amplitude and slope of the signal on magnetic field strength and the pump beam power is important for the cooling transition $F = 2 \rightarrow F' = 3$ transition of ^{87}Rb atoms.

Figure 6 shows the effect of magnetic field on (a) the amplitude and (b) slope of TDFDL signal for different values of the pump beam power. The TDFDL signal is 12 MHz red detuned from $F = 2 \rightarrow F' = 3$ transition of ^{87}Rb . The amplitude of the signal increases up to a field of 20 G and then starts to decrease. The slope of the signal initially increases with magnetic field and then achieves its maximum value of ~ 43 mV/MHz for the pump power of 1.13 mW and applied magnetic field of ~ 9.7 Gauss. A reduction in slope is observed for magnetic fields larger than ~ 9.7 G as the separation between σ_+ and σ_- transitions for the probe absorptions becomes more than a few natural widths. Therefore, it is evident from the graph that optimized slope and a large amplitude of TDFDL signal is obtained for the magnetic field of ~ 9.7 G and the pump beam power of 1.13 mW. The slope and the amplitude reduces significantly due to power broadening at the pump beam power greater than 1.13 mW. The behaviour of calculated TDFDL signal's amplitude and slope with magnetic field is similar to the experimental results. However, the optimum value of magnetic field (~ 9.7 Gauss) for the

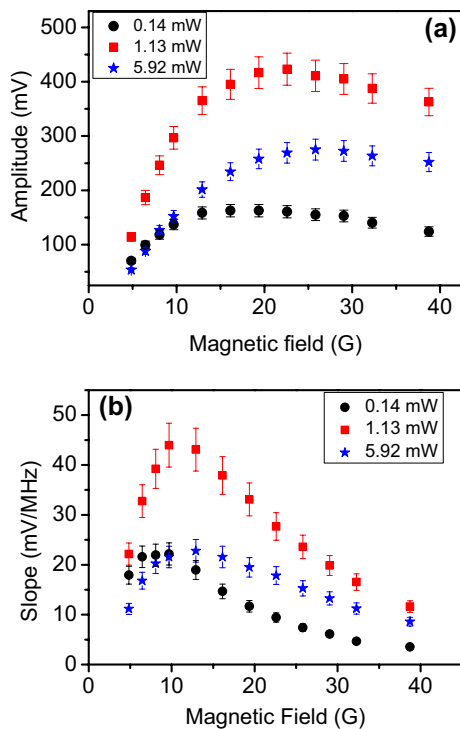


Fig. 6 Dependence of **a** amplitude and **b** slope of the TDFDL signal on magnetic field for $F = 2 \rightarrow F' = 3$ transition of ^{87}Rb atom. The data are recorded for probe laser beam power of $140 \mu\text{W}$ and for different pump laser beam power. TDFDL signal is 12 MHz red detuned from $F = 2 \rightarrow F' = 3$ transition of ^{87}Rb . Error bars represent standard deviation obtained in data of repeated measurements

experimental TDFDL signal for $F = 2 \rightarrow F' = 3$ transition of ^{87}Rb is different from the value for the calculated signal as shown in Fig. 3b. This may be due to the reason that our calculations are based on simple two-level model, whereas the real atomic system consists of multiple sub-levels in ground as well as excited state.

4.3 Frequency stabilization of the laser using the TDFDL signal and its application to the Rb-MOT setup

The frequency stability of an ECDL laser system using TDFDL locking signal has been studied. A standard PID (Toptica, Germany) controller is used to lock the laser frequency. The TDFDL signal was fed to this PID controller to lock the laser frequency. The desired frequency was selected by setting the lock reference level equal to the signal level at that frequency. The laser system remained frequency locked for several hours during the course of experiments. The error signal after frequency locking is recorded on a calibrated photodiode.

Our proposed TDFDL technique has two advantages. First is robust locking due to use of a dispersive-like signal with

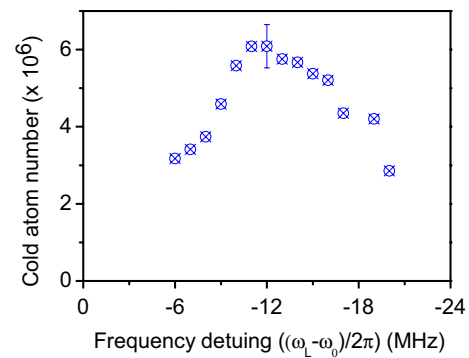


Fig. 7 The variation in maximum number of cold atoms in ^{87}Rb -MOT with detuning of cooling laser frequency using TDFDL locking method. The MOT is pulsed loaded using Rb dispenser with dispenser current of 7 A for 5 s duration. Error bar represents standard deviation obtained in data of repeated measurements

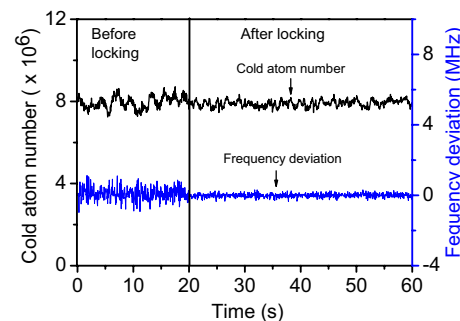


Fig. 8 The measured variation in number of cold atoms in the MOT and cooling laser frequency with time, before and after locking the laser frequency using TDFDL signal. The data are recorded with the probe laser beam power of $\sim 140 \mu\text{W}$ and with the pump laser beam power of $\sim 1.13 \text{ mW}$. The slope of TDFDL signal is $\sim 43 \text{ mV/MHz}$. The TDFDL signal was shifted $\sim 12 \text{ MHz}$ with respect to peak of the cooling transition of ^{87}Rb . For these measurements, a continuous MOT was operated by applying a dc current of $\sim 2.7 \text{ A}$ in the Rb dispenser

large slope, and second is large tunability without compromising the slope. The TDFDL signal has been used to lock the cooling laser frequency in the magneto-optical trap (MOT) setup. We can tune this cooling laser in locked condition itself, to precisely control the number of cold atoms in the MOT. The ^{87}Rb MOT is prepared in an octagonal chamber which is made of stainless steel with a residual pressure $\sim 1.4 \times 10^{-8}$ torr. The source of rubidium vapour used in this experiment is a SAES Rb metal dispenser. This dispenser is located at $\sim 19 \text{ cm}$ from the MOT centre. Two feed-through pins on which dispenser is mounted are connected to external current supply from outside the chamber. Six laser beams of $\sim 5 \text{ mW}$ power in each beam is used to form the MOT. The beam waist of each cooling laser beam is about $\sim 6 \text{ mm}$. The laser beam of an additional diode laser

is combined with that of the cooling laser for re-pumping of the atoms into the cooling transition. The quadrupole magnetic field gradient in axial direction was ~ 10 G/cm. The MOT was operated in pulsed mode. In this, a current of ~ 7 A is passed through Rb dispenser for 5 s duration and cooling laser frequency is changed using the TDFDL setup. Fluorescence signal of pulsed loaded MOT is recorded on a calibrated photodiode to measure the number in the MOT. In Fig. 7, the peak value of the number of atoms is plotted as a function of cooling laser detuning. The temperature of Rb dispenser is kept constant between each pulsed operation by flowing 1.5 A current to the dispenser. We have maintained ~ 5 min gap between each data. The precise control over laser frequency tuning using the TDFDL signal allowed the cooling laser detuning to be changed in steps of 1 MHz. We also note that the tuning was possible without breaking the frequency lock over a wide range. The cold atom number was found to be maximum ($\sim 6.0 \times 10^6$) at -12 MHz of cooling laser detuning. The atom cloud temperature is typically $\sim 300 \mu\text{K}$ for the values of cooling beam intensity and detuning used [29]. The result is in good agreement with the earlier work [31, 32].

Figure 8 shows the fluctuation in cooling laser frequency and the number of cold atoms in the MOT before and after locking the laser frequency. It is evident from this figure that both the number of cold atoms and the error signal (i.e. frequency deviation) show the significant reduction in the fluctuation after locking the laser frequency. Figure 8 shows that the fluctuation in number of cold atoms in the MOT gets reduced from $\sim \pm 10\%$ (before locking) to $\sim \pm 4.5\%$ (after locking), whereas the fluctuation in laser frequency gets reduced from $\sim \pm 1$ MHz (before locking) to $\sim \pm 0.25$ MHz (after locking). The laser is locked for more than 1 h.

5 Conclusion

In conclusion, a new laser frequency stabilization technique which we call as tunable Doppler-free dichroic lock (TDFDL) has been demonstrated. This technique provides a sharp and widely tunable dispersion-like signal useful for frequency locking of a laser. The amplitude and the slope of the signal depends on the pump beam power and the applied magnetic field. Using the TDFDL signal, the tuning of zero-crossing point in the TDFDL locking signal is achieved by varying the relative frequency difference between the pump and probe beams. The TDFDL signal has been utilized for the frequency locking and tuning of a laser used for the cooling of ^{87}Rb atoms in a magneto-optical trap.

Acknowledgments We are grateful to Amit Chaudhary for his help during the experimental work.

References

1. S. Chu, *Rev. Mod. Phys.* **70**, 685 (1998)
2. C.E. Wieman, L. Hollberg, *Rev. Sci. Instrum.* **1**, 62 (1991)
3. J.E.M. Goldsmith, E.W. Weber, T.W. Hnsch, *Phys. Rev. Lett.* **41**, 1525 (1978)
4. W. Demtroder, *Laser Spectroscopy*, 3rd edn. (Springer, Berlin, 1988)
5. K.B. MacAdam, A. Steinbach, C. Wieman, *Am. J. Phys.* **60**, 1098 (1992)
6. L. Mudarikwa, K. Pahwa, J. Goldwin, *J. Phys. B At. Mol. Opt. Phys.* **45**, 065002 (2012)
7. C. Wieman, W.T. Hansch, *Phys. Rev. Lett.* **36**, 1170 (1976)
8. C.P. Pearman, C.S. Adams, S.G. Cox, P.F. Griffin, D.A. Smith, I.G. Hughes, *J. Phys. B At. Mol. Opt. Phys.* **35**, 5141 (2002)
9. V.B. Tiwari, S. Singh, S.R. Mishra, H.S. Rawat, S.C. Mehendale, *Opt. Commun.* **263**, 249 (2006)
10. V.B. Tiwari, S. Singh, S.R. Mishra, H.S. Rawat, S.C. Mehendale, *Appl. Phys. B* **83**, 93 (2006)
11. Y.B. Kale, V.B. Tiwari, S. Singh, S.R. Mishra, H.S. Rawat, *J. Opt. Soc. Am. B* **31**, 2531 (2014)
12. L. Krzemien, K. Brzozowski, A. Noga, M. Witkowski, J. Zachorowski, M. Zawada, W. Gawlik, *Opt. Commun.* **284**, 1247 (2011)
13. S. Okubo, K. Iwakuni, T. Hasegawa, *Opt. Commun.* **285**, 4107 (2012)
14. W. Gawlik, *Acta Phys. Pol. A* **66**, 401 (1984)
15. U. Shim, J.A. Kim, W. Jhe, *J. Kor. Phys. Soc.* **35**, 222 (1999)
16. G. Wasik, W. Gawlik, J. Zachorowski, W. Zawadzki, *Appl. Phys. B* **75**, 613 (2002)
17. M.L. Harris, S.L. Cornish, A. Tripathi, I.G. Hughes, *J. Phys. B At. Mol. Opt. Phys.* **41**, 085401 (2008)
18. D.Q. Su, T.F. Meng, Z.H. Ji, J.P. Yuan, Y.T. Zhao, L.T. Xiao, S.T. Jia, *Appl. Opt.* **53**, 7011 (2014)
19. H. Liu, S. Yin, J. Qian, Z. Xu, Y. Wang, *J. Phys. B At. Mol. Opt. Phys.* **46**, 085005 (2013)
20. M. Miyabe, M. Kato, M. Oba, I. Wakaida, K. Watanabe, K. Wendt, *Jpn. J. Appl. Phys.* **45**, 4120 (2006)
21. G.W. Choi, H.R. Noh, *J. Phys. B At. Mol. Opt. Phys.* **48**, 115008 (2015)
22. K. Pahwa, L. Mudarikwa, J. Goldwin, *Opt. Express* **20**, 17456 (2012)
23. M. Pichler, C. David, *Opt. Commun.* **285**, 50 (2012)
24. T. Petelski, M. Fattori, G. Lamporesi, J. Stuhler, G.M. Tino, *Eur. Phys. J. D* **22**, 279 (2003)
25. K.L. Corwin, Z.-T. Lu, C.F. Hand, R.J. Epstein, C.E. Wieman, *Appl. Opt.* **37**, 3295 (1998)
26. A.M. Sicking, I.G. Hughes, P. Tierney, S.L. Cornish, *J. Phys. B At. Mol. Opt. Phys.* **40**, 187 (2007)
27. S. Imanishi, U. Tanaka, S. Urabe, *Jpn. J. Appl. Phys.* **44**, 6767 (2005)
28. N. Beverini, E. Maccioni, P. Marsili, A. Ruffini, F. Sorrentino, *Appl. Phys. B* **73**, 133 (2006)
29. V.B. Tiwari, S.R. Mishra, H.S. Rawat, S. Singh, S.P. Ram, S.C. Mehendale, *Pramana J. Phys.* **65**, 403 (2005)
30. G.W. Choi, H.R. Noh, *Opt. Commun.* **367**, 312 (2016)
31. K. Lindquist, M. Stephens, C. Wieman, *Phys. Rev. A* **46**, 4082 (1992)
32. J.P. McGilligan, P.F. Griffin, E. Riis, A.S. Arnold, *Opt. Express* **23**, 8948 (2015)